Dyes and Pigments 188 (2021) 109159

Contents lists available at ScienceDirect

Dyes and Pigments

journal homepage: http://www.elsevier.com/locate/dyepig

Study of the pyridyl-containing charge-trapping functional materials in the organic field effect transistor memory devices

Chaoyue Zheng, Yihong Huan, Chao Tan, Deqing Gao *

Key Laboratory of Flexible Electronics & Institute of Advanced Materials, Jiangsu National Synergistic Innovation Center for Advanced Materials, Nanjing Tech University, Nanjing, Jiangsu, 211816, PR China

ARTICLE INFO

Keywords:
Nonvolatile organic transistor memory
Hydrogen bonding
Aggregate
SAMs
Memory window

ABSTRACT

Interface materials can effectively improve the storage characteristics of the memory devices. In this paper, a series of functional materials with propyl chain bridging pyridyl ring and triethoxysilyl group, 3-(3-(triethoxysilyl)propyl)pyridine (Pyridyl-C), N-(3-(triethoxysilyl)propyl)pyridin-3-amine (Pyridyl-N) and 3-(3-(triethoxysilyl)propoxy)pyridine (Pyridyl-O), were selected as the charge-storage interface materials to study the storage characteristics of nonvolatile organic field-effect transistor (OFET) memory devices. The results demonstrated that the memory performance could be enhanced by adding lone-pair-electron atoms (N, O) between pyridyl group and propyl chain. With the programming voltage of −30 V staying in dark condition for 1 s, the memory windows were increased from 12.48 V to 14.95 V, then to 21.99 V when the –O and N atoms were introduced, respectively. All memory devices could remain stable for more than 10^4 s. The morphology images indicated that there were aggregates on the interfacial layers, and the size was increased when the atoms (O, N) were added because of the hydrogen-bonding interaction. The aggregates can increase the contact area between pentacene and interface materials and further enlarge the effective tunneling area. In addition, the variation of self-assembling immersing time for preparing Pyridyl-N layers was studied, indicating that with the extension of the immersing time, the size of aggregates was increasingly enlarged and memory performance was improved correspondingly.

1. Introduction

As an important component of information industry, memory device is an indispensable part of modern electronic products. Nonvolatile OFET memory devices, as a type of information storage, has potential applications in sensors [1,2], integrated organic device circuits [3,4] and smart memory cards [5] because of their affordability and flexible preparation [6]. Generally speaking, in order to store the information in the OFET memory device, an additional storage layer is required between the semiconductor layer and the gate dielectric so that the threshold voltage (V_{th}) can be controlled to shift [7]. Self-assembling monolayers (SAMs) are an effective strategy for interface engineering which can modify the surface of materials, such as oxides, metals, H-passivated Si etc. [6,8] The self-assembling molecules usually consist of three parts: anchor group (phosphonic acid for AlO_x or HfO_2 and organosilane precursors for SiO_2), alkyl chain and functional core group. It is worth noting that, in terms of SiO_2 surface, the development of strong Si–O–Si bonds between the precursor silane and surface silanol (-Si-OH) serves as a driving force to form SAMs [8]. The work functions of anode and cathode can be effectively adjusted by SAMs to improve the hole or electron mobility [9,10]. Octadecyltrichlorosilane (OTCS) is a commonly used material to modify the gate dielectrics in OFET. By applying the SAMs to the OFET, the field-effect mobility and the on/off current ratio are significantly improved [11]. For nonvolatile OFET memory devices, SAMs can be used not only as the charge trapping layer [4,12,13], but also as the interface layer [14].

In this paper, a series of charge-trapping molecules, Pyridyl-C, Pyridyl-N and Pyridyl-O, were studied. As shown in Fig. 1, all the three charge-trapping molecules contained the pyridyl group. The difference was that N and O atoms were inserted between the pyridyl group and the propyl chain for Pyridyl-N and Pyridyl-O, respectively. In order to highlight the performance of the target materials, triethoxy (3-phenylpropyl)silane (phenyl-C) was designed as the reference considering that it does not form the hydrogen bonding. By comparing the different atoms directly linking to the pyridyl, the effect of hydrogen-bonding interaction on the size of aggregates and the device performance was

* Corresponding author.
E-mail address: iamdqgao@njtech.edu.cn (D. Gao).

https://doi.org/10.1016/j.dyepig.2021.109159
Received 15 December 2020; Received in revised form 13 January 2021; Accepted 13 January 2021
Available online 17 January 2021

discussed in detail. The memory performance was enhanced when Pyridyl-N and Pyridyl-O were utilized as the interfacial layers. In addition, the effects of different self-assembling immersing time (10 s, 60 s, 10 min, 1 h, 20 h and 60 h) on the devices were discussed, showing that the size of aggregates was increased with the extension of immersing time and the corresponding memory window was increased.

2. Results and discussion

2.1. Synthesis

The functional materials were synthesized by following the synthetic routes in Scheme 1 in SI. For the three charge-trapping materials, the synthesis was completed by a two-step reaction. For Pyridyl-C, 3-pyridyl bromide and allyl bromide underwent an exchange reaction of Grignard reagent in the presence of i-PrMgCl-LiCl (isopropylmagnesium chloride-lithium chloride complex) to yield the intermediate of 3-allylpyridine with yield of 49.6%, and then a hydrosilylation reaction was carried out between 3-allylpyridine and triethoxysilane under Karstedt's catalyst with yield of 50%. For Pyridyl-N, the first step was the coupling reaction of 3-pyridyl bromide and allylamine with K_3PO_4 and CuI with yield of 80% and the second step was the similar hydrosilylation reaction with N-allylpyridin-3-amine as the starting material with yield of 40%. The synthesis of Pyridyl-O was completed firstly through the nucleophilic substitution reaction between 3-hydroxypyridine and allyl bromide with yield of 40% and then the hydrosilylation reaction with 3-(allyloxy)pyridine as the starting material with yield of 65%. Phenyl-C was obtained by one step with allylbenzene as the staring material with yield of 60%.

2.2. UV/vis absorption

UV/vis absorption spectrums of the three charge-trapping materials and the reference were showed in Fig. 1b. The absorption maxima were found at 260.2, 261.0, 250.1 and 277.1 nm for Phenyl-C, Pyridyl-C, Pyridyl-N and Pyridyl-O, respectively. It is noted that Pyridyl-N and Pyridyl-O presented obvious red-shift phenomenon, especially Pyridyl-N had an absorption at 310.0 nm; being attributed to the enlargement of conjugated system by the linked electron-donating N and O atoms [15].

2.3. Characterization of the charge-trapping layers and the pentacene layers

The molecular layers of the reference and the three charge-trapping materials were formed on the substrate of SiO_2 (50 nm)/Si by immersing the substrates into the toluene solution in 3 mM of Phenyl-C, Pyridyl-C, Pyridyl-N and Pyridyl-O respectively under 80 °C after the substrate was treated by oxygen plasma. In order to observe the charge-trapping layers, we first employed XPS, a preferable method, to study the surface [16]. Fig. 2a–c and Fig. S1 were the C (1s) peaks of the reference and the three charge-trapping layers. The characteristic C (1s) peak from C–Si was observed at 284.2 eV [16], while those from both C–H and C–C were at 284.8 eV [17]. It was noted that the C (1s) from C–N peaked at 285.5 eV in the pyridyl ring and the peak became broader in case of Pyridyl-N with a second N atom linked to the pyridyl ring besides the N atom in the pyridyl ring [16]. The C (1s) from the C–O was found at 286.3 eV in case of Pyridyl-O with O atom directly linked to the pyridyl ring [17]. Fig. 2d–f showed the N (1s) peaks of the corresponding layers. For Pyridyl-C and Pyridyl-O, the N atom of pyridyl ring could form hydrogen bonds, and the peaks at 398.9 eV and 399.9 eV corresponded to N (1s) from the pyridyl ring and hydrogen bond, respectively [18]. It was observed that the peak area of 399.9 eV was larger than that of

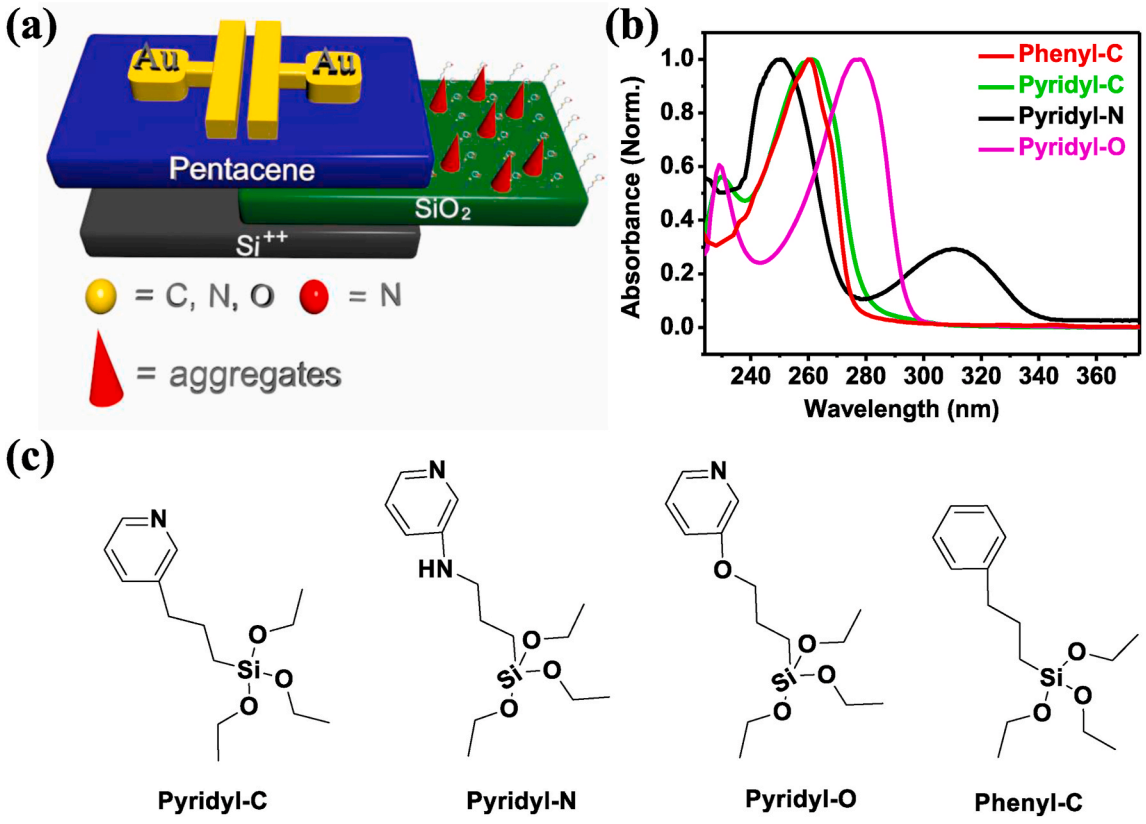

Fig. 1. (a) Schematic diagram of OFET memory device, (b) UV/vis absorption spectrum of four materials and (c) Chemical structures of Pyridyl-C, Pyridyl-N, Pyridyl-O and Phenyl-C.

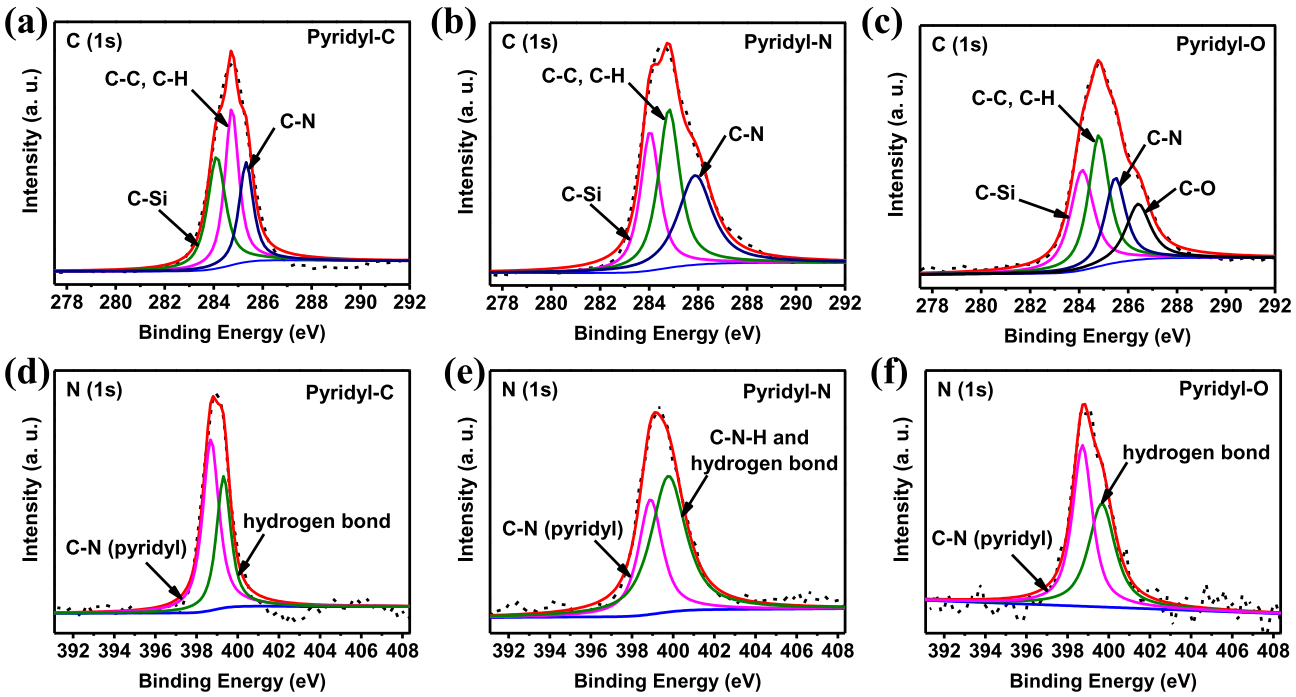

Fig. 2. XPS: C (1s) and N (1s) binding-energy peaks of three materials on SiO_2: Pyridyl-C (a, d), Pyridyl-N (b, e) and Pyridyl-O (c, f).

398.9 eV in the case of Pyridyl-N. The reason is that the N atom linked on the ring and its hydrogen bond made more contribution, compared with the hydrogen bond of the pyridyl N atom [19]. The result of XPS indicated the formation of multilayers due to hydrogen bonding from N atoms on the molecular structure.

Water contact angle measurements of the reference and the charge-trapping layers were studied (Fig. 3). The water contact angles of Phenyl-C, Pyridyl-C, Pyridyl-N and Pyridyl-O layers were 60.5°, 74.2°, 89.0° and 75.7°, respectively, indicating different hydrophobicity of the layers. The layers of the Pyridyl-containing materials delivered higher hydrophobicity property than Phenyl-C layer. Morphology had an important influence on the performance of the OFET memory devices. The AFM topographic images of the reference and the charge-trapping layers were shown in Fig. 3a–d. The Phenyl-C layer was smooth with few aggregates in Fig. 3a. In contrast, when the benzene ring was replaced by the pyridyl ring, the aggregates with a size of approximately 180–200 nm were found on the Pyridyl-C layer. The aggregates became bigger when the auxochromes (–NH– or -O-) were linked to the pyridyl ring, about 450–600 nm on the Pyridyl-N layer and 250–390 nm on the Pyridyl-O layer. Different sizes of aggregates were formed during the self-assembling process on the substrates. As shown in Fig. 4, the triethoxysilyl group evoked the hydrolysis reaction and then the Si–O–Si

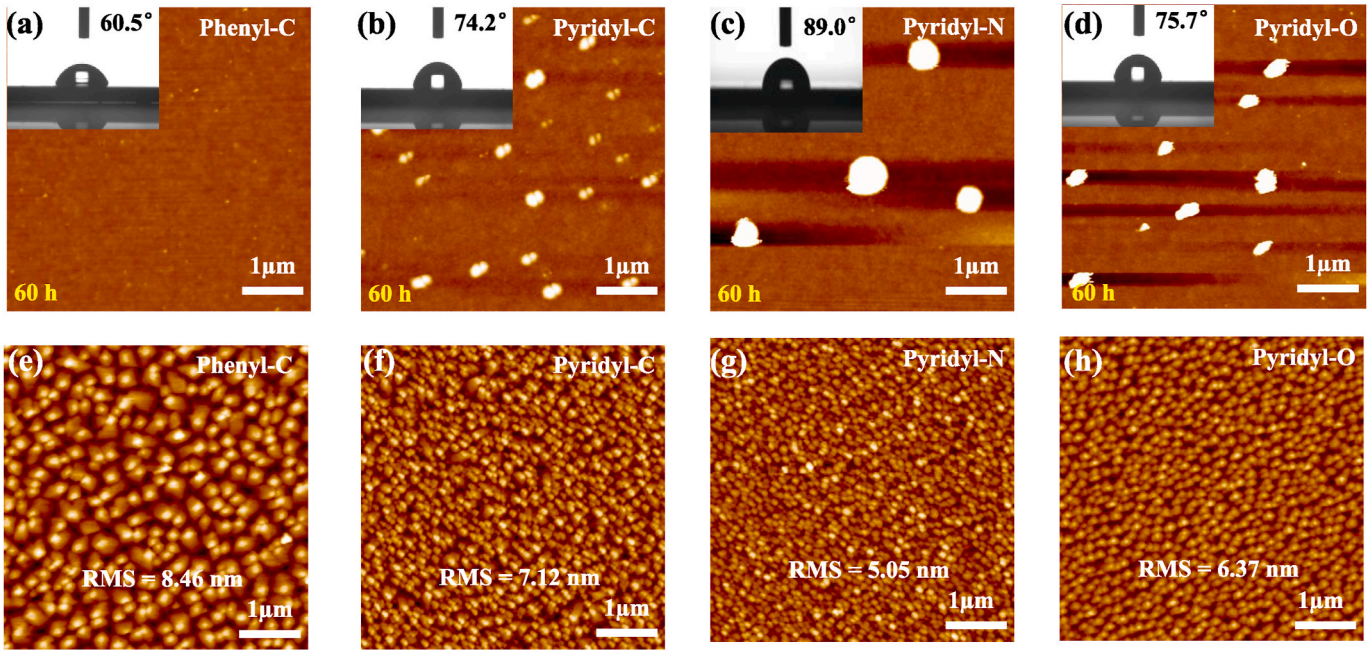

Fig. 3. AFM topographic images and water contact angles of the reference and charge-trapping layers: (a) Phenyl-C; (b) Pyridyl-C; (c) Pyridyl-N and (d) Pyridyl-O. Pentacene films in 50 nm deposited above the reference and charge-trapping layers of Phenyl-C (e), Pyridyl-C (f), Pyridyl-N (g) and Pyridyl-O (h).

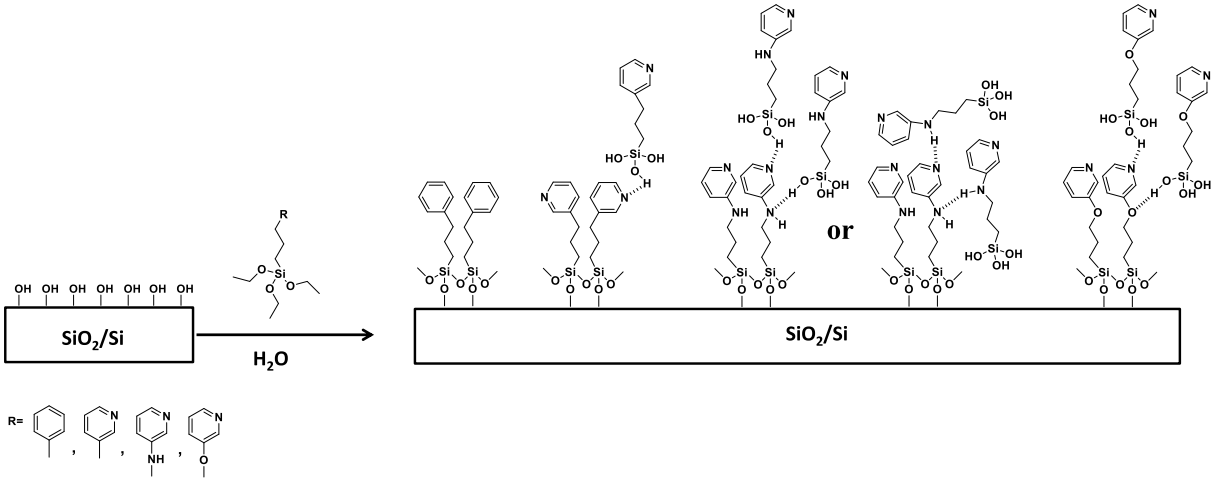

Fig. 4. Molecular arrangement corresponding to the layer of Phenyl-C, Pyridyl-C, Pyridyl-N or Pyridyl-O on SiO_2 substrates prepared from self-assembling process in which hydrogen bonding is involved in the case of Pyridyl-C, Pyridyl-N and Pyridyl-O.

bonds were formed between surface's hydroxyl group and the hydrolyzed triethoxysilyl group. The aggregates for Pyridyl-C were formed because of the hydrogen bonding between the hydrolyzed triethoxysilyl group and the N atom from the pyridyl ring [20,21]. As the auxochromes (–NH–, -O-) linked to the pyridyl ring could form the hydrogen bonding with the hydrolyzed triethoxysilyl group as well, the size of aggregates for Pyridyl-N and Pyridyl-O appeared larger than those for Pyridyl-C. Pyridyl-N offered NH group to form hydrogen bonds with the pyridyl ring and by itself. It had the largest aggregates on the layer surface.

The growth and crystallization of the pentacene layers were affected by the self-assembling layers. When the surface was rough, the activation energy for the nucleation and re-evaporation of pentacene was small [22,23]. As shown in Fig. 3e–h, when the SiO_2 was modified by the reference and the charge-trapping layers respectively, different morphologies of pentacene layers were observed. The grain size of pentacene film above the Phenyl-C layer appeared to be the largest while the smallest above the Pyridyl-N layer. The root-mean-square roughness (R_q) values of pentacene films were in the decreasing order of 8.46 nm, 7.12 nm, 6.37 nm and 5.05 nm with the Phenyl-C, Pyridyl-C, Pyridyl-O and Pyridyl-N underlayers, respectively. That is, with increasing size of the aggregates and water contact angles in the order of Phenyl-C, Pyridyl-C, Pyridyl-O and Pyridyl-N underlayers, the corresponding pentacene film was smoother. This observation reflects the synergic action of surface roughness and wetting property of the underlayers on film formation of the above-deposited pentacene, in agreement with the report [22,23].

2.4. Electrical characteristics of OFET memory devices

The electrical characteristics of the reference and the charge-trapping devices were carried out. Fig. S3-S4 demonstrated the typical p-type behavior with the current increasing when the gate bias was scanned from positive value to negative value. The results of field-effect mobility (μ_{FET}), the on/off current ratio (I_{on}/I_{off}) and the threshold voltage (V_{th}) of four devices were displayed in Table 1. The field-effect mobility of all the three charge-trapping devices was lower when compared with the Phenyl-C device. The mobility of Pyridyl-C device and Pyridyl-O device was 0.031 ± 0.002 $cm^2\ V^{-1}\ s^{-1}$ and 0.016 ± 0.002 $cm^2\ V^{-1}\ s^{-1}$, respectively, while that of Pyridyl-N device was only 0.0032 ± 0.0006 $cm^2\ V^{-1}\ s^{-1}$. Different mobility could be explained by the various morphologies of pentacene films (Fig. 3e–h). It seems that the bigger the grain size of pentacene is, its mobility is the higher, in agreement with the literature [24]. The size of pentacene grain above the Pyridyl-N layer was the smallest, and the mobility was the lowest.

Table 1
Characteristics of the transistor and memory performance for four devices.

Devices	μ_{FET} ($cm^2\ V^{-1}\ s^{-1}$)	V_{th} (V)	I_{on}/I_{off}	Memory window (V)	Δn [cm^{-2}]
Phenyl-C	0.43 ± 0.03	−4.25	3.99×10^4	0	0
Pyridyl-C	0.031 ± 0.002	−4.02	1.08×10^5	12.48	5.15×10^{12}
Pyridyl-N	0.0032 ± 0.0006	−0.05	2.41×10^3	21.99	9.07×10^{12}
Pyridyl-O	0.016 ± 0.002	−1.68	2.26×10^4	14.95	6.17×10^{12}

In order to study the storage capability of the three charge-trapping devices with different hydrogen-bonding interaction in detail, the reversible threshold voltage shifts were applied. The programming operation was carried out with V_{GS} of −30 V staying in dark for 1 s and the erasing process was operated by employing the light illumination [25] for 1s with the wavelength of 400–700 nm and the light intensity of 15 mW cm^{-2}. In order to illustrate the storage performance of the three charge-trapping devices with different hydrogen-bonding interaction, the memory window of Phenyl-C device without hydrogen-bonding interaction acted as the reference device. Fig. 5 showed the results of memory window of the three charge-trapping devices and the reference device, respectively. Except the reference device, all the threshold voltages were shifted to the negative side with the programming operation of −30 V, indicating that the hole carriers were trapped. The reference device had almost no memory window. The memory window of 21.99 V from the Pyridyl-N device was the largest among four devices, presenting the strongest ability of capturing hole carriers, followed by 14.95 V from Pyridyl-O device and 12.48 V from Pyridyl-C device. Though the memory window of Pyridyl-C was smaller, the storage efficiency (the ratio between the memory window and the programming voltage) of it exceeded 1/3. The results illustrated that the pyridyl group had a stronger ability of trapping hole carriers compared with the reference device.

The charge-storage density (Δn) can be calculated by the following equation[23]

$$\Delta \mathbf{n} = \frac{\Delta V_{th}}{e} C_i$$

Where C_i represents the total capacitance per unit area and e is the elementary charge. By calculation, the Δn values were about 0, 5.15×10^{12}, 9.07×10^{12} and 6.17×10^{12} for Phenyl-C, Pyridyl-C, Pyridyl-N

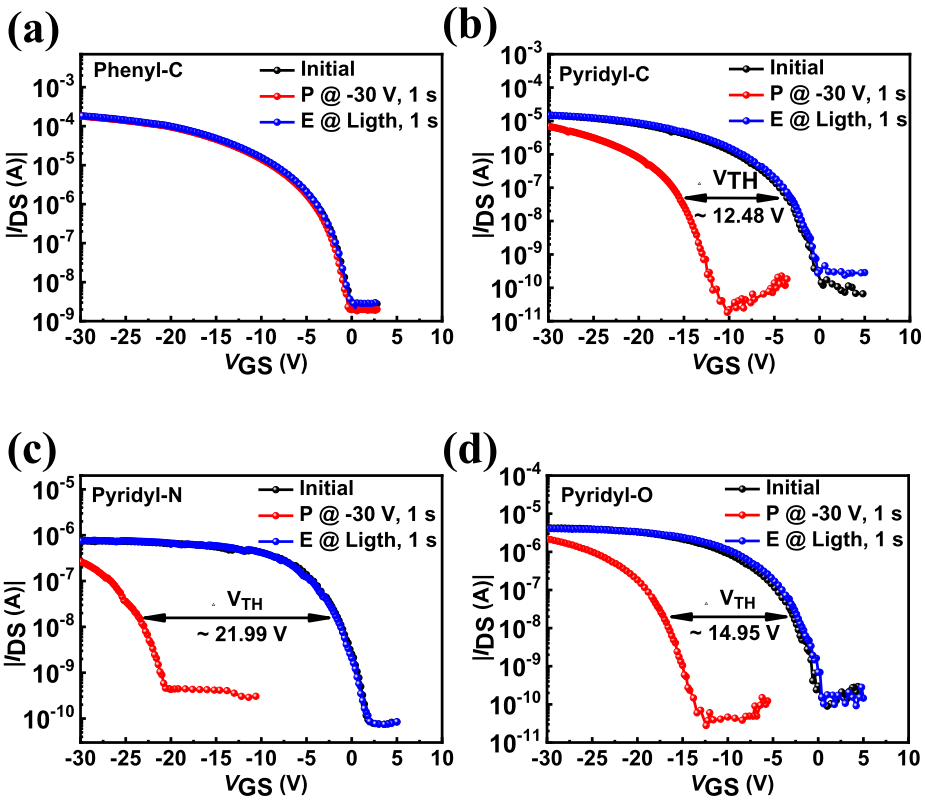

Fig. 5. Typical memory windows of threshold voltage shifts for the OFET memory devices in electrical programming and light erasing operation mode: (a) Phenyl-C; (b) Pyridyl-C; (c) Pyridyl-N and (d) Pyridyl-O.

and Pyridyl-O layers, separately. The data were compiled in Table 1. The results showed that more charges can be trapped by Pyridyl-N device.

Taking into account the HOMO energy levels, as shown in Fig. S5a, the HOMO energy levels were −5.35 eV for Pyridyl-C, −5.18 eV for Pyridyl-N and −5.38 eV for Pyridyl-O. Since the HOMO energy level barriers between pentacene and the pyridyl molecules showed no significant difference, it could be concluded that the different memory windows of the three charge-trapping devices with pyridyl group were related to the interface between self-assembling films and pentacene. For Pyridyl-N device, the aggregates whose size was the largest on the charge-trapping layer would increase the contact area between pentacene and Pyridyl-N molecules, contributing to the expansion of the effective tunneling area and more charges being injected [23,26]. Pyridyl-C layer presented the smallest aggregates and the device delivered the narrowest memory window. It was worth noting that there were few aggregates on the Phenyl-C film and the corresponding device had almost no memory window, proving that aggregates had an important impact on the storage performance.

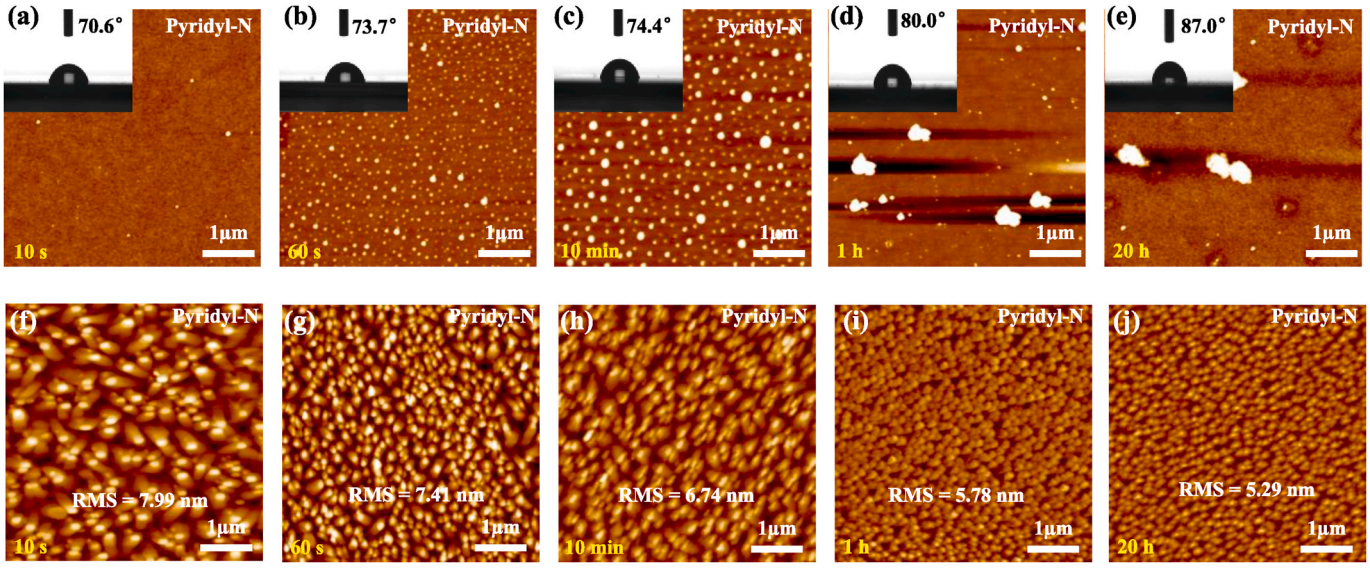

Fig. 6. AFM topographic images and water contact angles of Pyridyl-N layers in various immersing time: (a) 10 s, (b) 60 s, (c) 10 min, (d) 1 h and (e) 20 h 50 nm pentacene deposited above the corresponding Pyridyl-N layers.

To explore the influence of the aggregates on memory properties, a series of aggregates of various sizes on Pyridyl-N layers were prepared by adjusting the immersing time in the self-assembling process [27]. The immersing time was 10 s, 60 s, 10 min, 1 h, 20 h and 60 h, respectively. Fig. 6a–e showed the morphology images and water contact angles of Pyridyl-N layers with different immersing time lengths. Small aggregates were found in 10 s, suggesting pretty quick formation of the aggregates. With the immersing time increasing, the aggregates became larger, the corresponding water contact angle was increased from 70.6° from 10 s to 87.0° from 20 h, even 89° from 60 h (Fig. 3c), and the layer became more hydrophobic. Interestingly, the pentacene films above the layers presented different morphologies. The size of pentacene grain was getting smaller above the Pyridyl-N layer with the increasing size of aggregates (Fig. 6f–j), being well in agreement with the previously observed behaviour of pentacene film above the Phenyl-C, Pyridyl-C, Pyridyl-N and Pyridyl-O layers (Fig. 3).

The corresponding memory devices were fabricated and characterized. As shown in Fig. 7 and Table 2. The memory window and charge-storage density became larger with the extending immersing time, 4.14 V and 1.71×10^{12} from 10 s, 6.53 V and 2.69×10^{12} from 60 s, 9.78 V and 4.03×10^{12} from 10 min, 17.45 V and 7.20×10^{12} from 1 h, 19.44 V and 8.02×10^{12} from 20 h, and 21.99 V and 9.07×10^{12} from 60 h, respectively. It is clear that the size of aggregates of the charge trapping layers affected the pentacene film and further affected the memory performance. The mobility of the devices was also various. As compiled in Table 2, the mobility was getting lower and lower when the immersing time continued to be extended [23].

In order to further test the endurance characteristics of the three charge-trapping devices, write-read-erase-read (WRER) cycles were employed. The results were showed in Fig. 8a–c. The WRER cycles were conducted in dark, with the writing gate voltage of −30 V and −10 V for reading gate voltage and with the erasing process by employing the light illumination in the absence of gate voltage. The rewritable memory characteristics of all the three charge-trapping devices could remain stable without almost any decay with 150 continuous writing, reading and erasing cycles. In order to estimate the charge storage stability of the three charge-trapping devices, the retention characteristics was measured by the writing gate voltage of −30 V and −10 V for reading gate voltage. The results were showed in Fig. 8d–f. All the three charge-trapping devices presented rapid ON-current decay and OFF-current increasing at the initial stage. Afterwards, the ON-current and the OFF-current were stable.

Table 2
Characteristics of the OFET memories with the self-assembled Pyridyl-N layers prepared in various immersing time.

Time	μ_{FET} ($cm^2 V^{-1} s^{-1}$)	V_{th} (V)	I_{on}/I_{off}	Memory window (V)	Δn [cm^{-2}]
10 s	0.084 ± 0.001	−3.22	3.04×10^4	4.14	1.71×10^{12}
60 s	0.051 ± 0.003	−3.10	3.20×10^4	6.53	2.69×10^{12}
10 min	0.039 ± 0.003	−3.04	1.12×10^5	9.78	4.03×10^{12}
1 h	0.0086 ± 0.0006	−3.79	2.08×10^3	17.45	7.20×10^{12}
20 h	0.0043 ± 0.0004	−0.92	6.63×10^3	19.44	8.02×10^{12}
60 h	0.0032 ± 0.0006	−0.05	2.41×10^3	21.99	9.07×10^{12}

3. Conclusions

In conclusion, the three charge-trapping materials based on pyridyl derivatives were studied for OFET memory devices. Due to strong hydrogen bonding, Pyridyl-N layer was covered with the largest aggregates, and the corresponding OFET memory device showed the biggest memory window (21.99 V) with the programming voltage of −30 V staying in dark for 1 s, followed by the Pyridyl-O device (14.95 V) and the Pyridyl-C device (12.48 V). In addition, different self-assembling immersing time for preparing Pyridyl-N layers was studied, indicating the size of aggregates and memory windows could be enhanced gradually as the immersing time was extended.

4. Experimental section

4.1. Materials and instruments

Allylbenzene (98%), platinum (0)-1,3-divinyl-1,1,3,3-

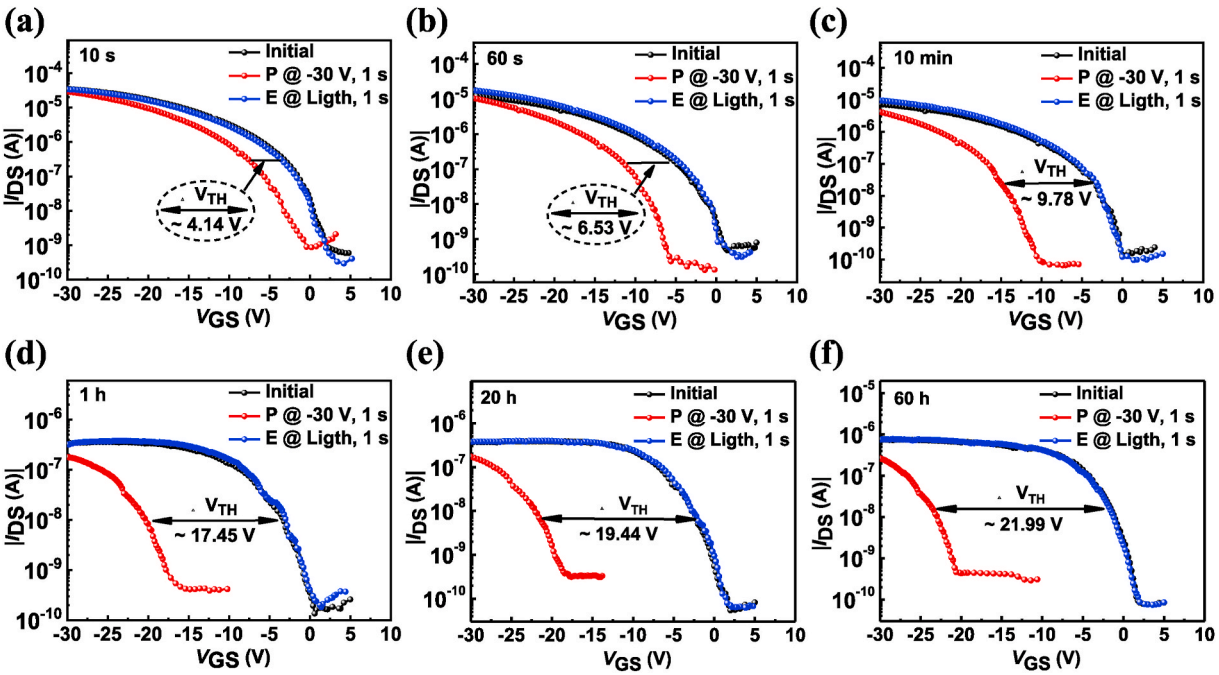

Fig. 7. Memory windows with Pyridyl-N layers prepared in various immersing time: (a) 10 s, (b) 60 s, (c) 10 min, (d) 1 h, (e) 20 h and (f) 60 h.

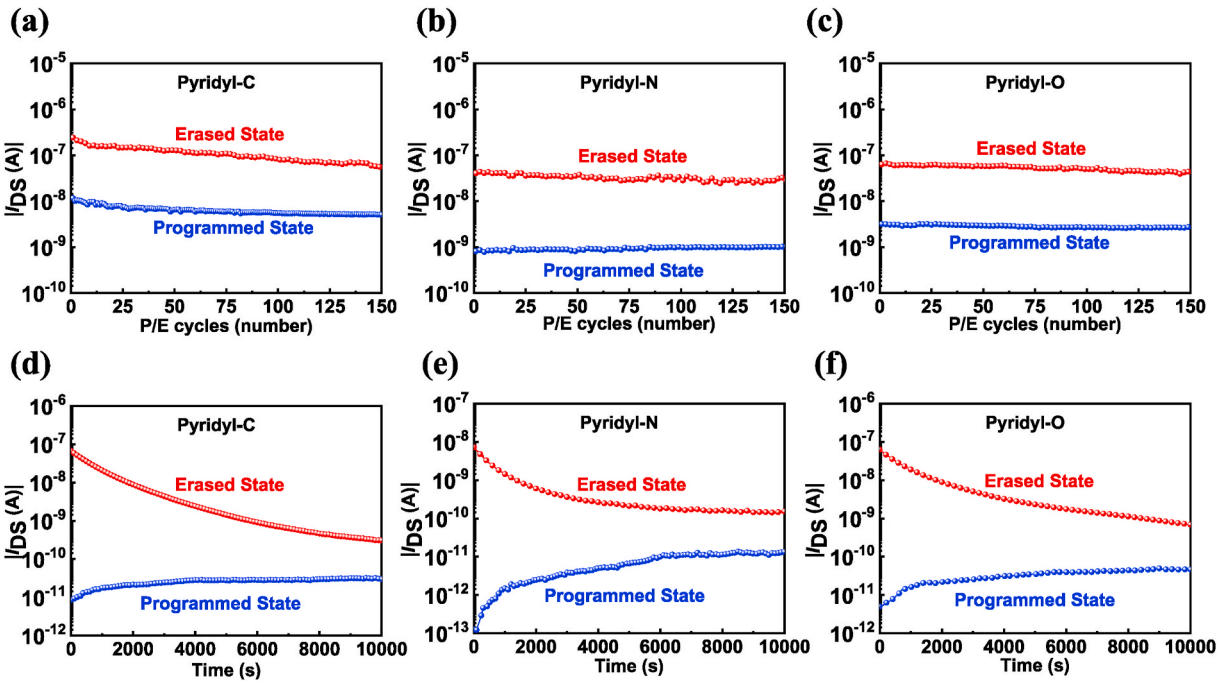

Fig. 8. Endurance characteristics cycles of OFET memory devices. The writing, reading, and erasing voltages were at V_{GS} = −30 V, −10 V, and 0 V (Light), respectively: (a) Pyridyl-C device; (b) Pyridyl-N device and (c) Pyridyl-O device. Retention characteristics of OFET memory devices: (d) Pyridyl-C device; (e) Pyridyl-N device and (f) Pyridyl-O device.

tetramethyldisiloxane (in xylene, Pt ~2%) (Karstedt's catalyst), triethoxysilane (97%), isopropylmagnesium chloride complex (*i*-PrMgCl-LiCl, 1.3 M THF solution), 3-pyridyl bromide (98%), allyl bromide (98%), potassium phosphate (98%) and 3-hydroxypyridine (99%) were purchased from Energy Chemical. L-proline and copper(I) iodide (99.5%) were purchased from Sinopharm Chemical Reagent Co., Ltd. Allylamine (98%) was purchased from Xiya Reagent. All of them were used without any further purification. Nuclear magnetic resonance (NMR) (500 MHz) spectra were recorded on Bruker AMX400 spectrometer in $CDCl_3$. HRMS-(ESI-TOF) was measured on AGILENT 1260–6230 TOF LC-MS. UV/vis spectra were recorded on Shimadzu UV-1750. The surface morphology of pentacene was investigated by using an XE-70 atomic force microscope (AFM) operating in tapping mode. The electrical characteristics of the memory devices were characterized by keithely 4200 semiconductor parameter analyzer.

4.2. Synthetic procedures

4.2.1. 3-Allylpyridine

According to the literature [28], to a 25 mL two-necked round bottom flask, 1.57 g of 3-pyridyl bromide (10 mmol) in dry THF (10 mL) and 15 mL of *i*-PrMgCl-LiCl were added dropwise under nitrogen at 0 °C. The mixture was stirred for 6 h under 0 °C and 4.76 g of allyl bromide (40 mmol) was added. After the mixture was slowly warmed to room temperature and kept stirring for 15 h, saturated NH_4Cl was added and the resulting mixture was extracted with ethyl acetate. The combined organic layers were dried over anhydrous $MgSO_4$ and filtrated, and the solvent was removed under reduced pressure. The crude product was purified by column chromatography on silica gel with petroleum ether/ethyl acetate (1:1, v/v) as the eluent. The collected yellow oil was concentrated to get the product (590 mg, 49.6% yield). ^{1}H NMR (500 MHz, $CDCl_3$): δ 8.45 (m, 2H), 7.50 (m, 1H), 7.22 (m, 1H), 5.94 (m, 1H), 5.11 (m, 2H), 3.38 (d, J = 5.0 Hz, 2H). ^{13}C NMR (126 MHz, $CDCl_3$): δ 150.11, 147.67, 136.31, 136.24, 135.49, 123.49, 116.96, 37.35.

4.2.2. 3-(3-(Triethoxysilyl)propyl)pyridine (Pyridyl-C)

To a dry schlenk flask, 238 mg of 3-allylpyridine (2 mmol), 656 mg of triethoxysilane (4 mmol) and 2.0 mg of Karstedt's catalyst were added in the absence of solvent under nitrogen and then the resulting mixture was placed at 80 °C for 20 h [29,30]. After cooling down to room temperature, the crude product was purified by column chromatography on silica gel with petroleum ether/ethyl acetate (3:1, v/v) as the eluent. The collected yellow oil was concentrated to get the product (283 mg, 50% yield). ^{1}H NMR (500 MHz, $CDCl_3$): δ 8.43 (m, 2H), 7.49 (m, 1H), 7.19 (m, 1H), 3.80 (q, J = 6.7 Hz, 6H), 2.64 (t, J = 7.5 Hz, 2H), 1.74 (m, 2H), 1.21 (t, J = 5.0 Hz, 9H), 0.65 (m, 2H). ^{13}C NMR (126 MHz, $CDCl_3$): δ 150.13, 147.31, 137.72, 136.14, 123.38, 58.53, 36.22, 24.73, 18.43, 10.25. HRMS-(ESI-TOF) for $C_{14}H_{25}NO_3Si$ $[M+H]^+$: calculated: 284.16765, found: 284.17035.

4.2.3. N-allylpyridin-3-amine

According to the literature [31], to a 25 mL two-necked round bottom flask, 1.57 g of 3-pyridyl bromide (10 mmol), 1.71 g of allylamine (30 mmol), 4.24 g of K_3PO_4 (20 mmol), 0.19 g of CuI (1 mmol) and 0.23 g of L-proline (2 mmol) in dry DMF (10 mL) were added under nitrogen. The mixture was stirred for 40 h under 80 °C. After cooling down to room temperature, the resulting mixture was extracted with ethyl acetate and water. The combined organic layers were dried over anhydrous $MgSO_4$ and filtrated, with the solvent being removed under reduced pressure. The crude product was purified by column chromatography on silica gel with petroleum ether/ethyl acetate (1:1, v/v) as the eluent. The collected yellow oil was concentrated to get the product (1.07 g, 80% yield). ^{1}H NMR (500 MHz, $CDCl_3$): δ 8.01 (m, 2H), 7.08 (m, 1H), 6.88 (m, 1H), 5.92 (m, 1H), 5.24 (m, 2H), 3.89 (s, 1H), 3.80 (m, 2H). ^{13}C NMR (126 MHz, $CDCl_3$): δ 144.26, 138.56, 136.15, 134.66, 123.88, 118.59, 116.63, 46.05.

4.2.4. N-(3-(Triethoxysilyl)propyl)pyridin-3-amine (Pyridyl-N)

To a dry schlenk flask, 268 mg of N-allylpyridin-3-amine (2 mmol), 656 mg of triethoxysilane (4 mmol) and 2.0 mg of Karstedt's catalyst were added in the absence of solvent under nitrogen and then the resulting mixture was placed at 80 °C for 20 h. After cooling down to room temperature, the crude product was purified by column chromatography on silica gel with petroleum ether/ethyl acetate (1:1, v/v) as

the eluent. The collected yellow oil was concentrated to get the product (238 mg, 40% yield). ^{1}H NMR (500 MHz, $CDCl_3$): δ 7.99 (m, 1H), 7.89 (m, 1H), 7.03 (m, 1H), 6.83 (m, 1H), 3.81 (m, 6H), 3.12 (t, J = 7.5 Hz, 2H), 1.72 (m, 2H), 1.20 (t, J = 7.5 Hz, 9H), 0.69 (m, 2H). ^{13}C NMR (126 MHz, $CDCl_3$): δ 144.50, 138.43, 136.10, 123.77, 118.39, 58.58, 45.99, 22.72, 18.39, 7.93. HRMS-(ESI-TOF) for $C_{14}H_{26}N_2O_3Si$ $[M+H]^+$: calculated: 299.17855, found: 299.18015.

4.2.5. 3-(Allyloxy)pyridine

According to the literature [32], to a 250 mL two-necked round bottom flask, 1.90 g of 3-hydroxypyridine (20 mmol), 3.86 g of K_2CO_3 (28 mmol) and 4.76 g of allyl bromide (40 mmol) and acetone (100 mL) were added. The mixture was stirred for 12 h under 75 °C. After cooling down to room temperature, the mixture was extracted with ethyl acetate and water. The combined organic layers were dried over anhydrous $MgSO_4$ and filtrated, and the solvent was removed under reduced pressure. The crude product was purified by column chromatography on silica gel with petroleum ether/ethyl acetate (3:1, v/v) as the eluent. The collected yellow oil was concentrated to get the product (1.08 g, 40% yield). ^{1}H NMR (500 MHz, $CDCl_3$): δ 8.34 (m, 1H), 8.23 (m, 1H), 7.22 (m, 2H), 6.04 (m, 1H), 5.41 (m, 2H), 4.59 (d, J = 10.0 Hz, 2H).

4.2.6. 3-(3-(Triethoxysilyl)propoxy)pyridine (Pyridyl-O)

To a dry schlenk flask, 270 mg of 3-(allyloxy)pyridine (2 mmol), 656 mg of triethoxysilane (4 mmol) and 2.0 mg of Karstedt's catalyst were added in the absence of solvent under nitrogen before the resulting mixture was placed at 80 °C for 20 h. After cooling down to room temperature, the crude product was purified by column chromatography on silica gel with petroleum ether/ethyl acetate (3:1, v/v) as the eluent. The collected oil was concentrated to get the product (389 mg, 65% yield). ^{1}H NMR (500 MHz, $CDCl_3$): δ 8.29 (m, 1H), 8.18 (m, 1H), 7.17 (m, 2H), 3.98 (t, J = 10.0 Hz, 2H), 3.82 (q, J = 10.0 Hz, 6H), 1.89 (m, 2H), 1.21 (t, J = 10.0 Hz, 9H), 0.75 (m, 2H). ^{13}C NMR (126 MHz, $CDCl_3$): δ 155.38, 141.99, 138.22, 123.88, 121.22, 70.30, 58.57, 22.87, 18.40, 6.61. HRMS-(ESI-TOF) for $C_{14}H_{25}NO_4Si$ $[M+H]^+$: calculated: 300.16256, found: 300.16416.

4.2.7. Triethoxy(3-phenylpropyl)silane (Phenyl-C)

To a dry schlenk flask, 236 mg of allylbenzene (2 mmol), 656 mg of triethoxysilane (4 mmol) and 2.0 mg of Karstedt's catalyst were added in the absence of solvent under nitrogen before the resulting mixture was placed at 80 °C for 20 h. After cooling down to room temperature, the crude product was purified by column chromatography on silica gel with petroleum ether/ethyl acetate (15:1, v/v) as the eluent. The collected pale yellow oil was concentrated to get the product (340 mg, 60% yield). ^{1}H NMR (500 MHz, $CDCl_3$): δ 7.27 (m, 2H), 7.17 (m, 3H), 3.80 (q, J = 6.7 Hz, 6H), 2.65 (t, J = 7.5 Hz, 2H), 1.75 (m, 2H), 1.20 (t, J = 7.5 Hz, 9H), 0.68 (m, 2H). ^{13}C NMR (126 MHz, $CDCl_3$): δ 142.58, 128.68, 128.36, 125.81, 58.49, 39.36, 24.95, 18.43, 10.34. HRMS-(ESI-TOF) for $C_{15}H_{26}O_3Si$ $[M+H]^+$: calculated: 283.1724, found: 283.17377.

4.3. Preparation of self-assembling layers and OFET memory devices

The OFET memory devices employed the typical structure of bottom gate/top contact [33]. The substrate was the heavily-doped n-type Si wafer and 50 nm SiO_2 as the gate insulator layer on the Si wafer. The SiO_2/Si substrates was treated in acetone, ethanol and deionized water for 5 min under the ultrasonic atmosphere, respectively; and then the substrates were dried in the oven for 30 min at 100 °C. The 3 mM solutions of the three charge-trapping materials (Pyridyl-C, Pyridyl-N and Pyridyl-O) and the reference material (Phenyl-C) in toluene were prepared, respectively. The substrates were immersed in the solution for 60 h at 80 °C after it was treated by oxygen plasma for 10 min. The SAM-substrates were rinsed with dry toluene and put into the oven for 30 min at 110 °C. The semiconductor layer (50 nm) of pentacene was deposited onto the self-assembling layer by the thermal vacuume vaporation method with a deposite rate of 0.1 A/s under a pressure of 5 × 10^{-4} Pa. Finally, 50 nm Au was deposited onto the pentacene layer as the source and drain electrodes with the channel width of 2000 μm and the channel length of 100 μm.

Declaration of competing interest

There are no conflicts to declare.

Acknowledgements

This work was supported by Natural Science Fundamental Research Project of Jiangsu Province's Colleges and Universities under grant No. 20KJA150012 and National Natural Science Foundation of China under grant No. 21371096.

Appendix A. Supplementary data

Supplementary data to this article can be found online at https://doi.org/10.1016/j.dyepig.2021.109159.

References

[1] Sekitani T, Yokota T, Zschieschang U, Klauk H, Bauer S, Takeuchi K, Takamiya M, Sakurai T, Someya T. Science 2009;326:1516.
[2] Mannsfeld SCB, Tee BCK, Stoltenberg RM, Chen CVHH, Barman S, Muir BVO, Sokolov AN, Reese C, Bao ZN. Nat Mater 2010;9:859.
[3] Kim SJ, Lee JS. Nano Lett 2010;10:2884.
[4] Chen HL, Cheng NY, Ma W, Li ML, Hu SX, Gu L, Meng S, Guo XF. ACS Nano 2016;10:436.
[5] Cho I, Kim BJ, Ryu SW, Cho JH, Cho JH. Nanotechnology 2014;25:505604.
[6] Ling HF, Liu SH, Zheng ZJ, Yan F. Small Methods 2018;2:1800070.
[7] Lv JJ, Gao X, Zhang LX, Feng Y, Xu JL, Xiao J, Dong B, Wang SD. Appl Phys Lett 2019;115:113302.
[8] DiBenedetto SA, Facchetti A, Ratner MA, Marks TJ. Adv Mater 2009;21:1407.
[9] Huang LQ, Chen L, Huang PR, Wu FY, Tan LC, Xiao SQ, Zhong W, Sun LX, Chen YW. Adv Mater 2016;28:4852.
[10] Mori T, Imanishi M, Nishikawa T. J Photopolym Sci Technol 2012;25:327.
[11] Walter SR, Youn J, Emery JD, Kewalramani S, Hennek JW, Bedzyk MJ, Facchetti A, Marks TJ, Geiger FM. J Am Chem Soc 2012;134:11726.
[12] Burkhardt M, Jedaa A, Novak M, Ebel A, Voïtchovsky K, Stellacci F, Hirsch A, Halik M. Adv Mater 2010;22:2525.
[13] Tseng CW, Huang DC, Tao YT. ACS Appl Mater Interfaces 2015;7:9767.
[14] Chang HC, Lee WY, Tai Y, Wu KW, Chen WC. Nanoscale 2012;4:6629.
[15] Ko YG, Kim DM, Kim K, Jung SM, Wi D, Michinobu T, Ree M. ACS Appl Mater Interfaces 2014;6:8415.
[16] Chong ASM, Zhao XS. J Phys Chem B 2003;107:12650.
[17] Zhuang JQ, Sun QJ, Zhou Y, Han ST, Zhou L, Yan Y, Peng HY, Venkatesh S, Wu W, Li RKY, Roy VAL. ACS Appl Mater Interfaces 2016;8:31128.
[18] Zeng XM, Chan CM, Weng LT, Li L. Polymer 2000;41:8321.
[19] Zhang ZY, Deng ZP, Zhang XF, Huo LH, Zhao H, Gao S. CrystEngComm 2014;16:359.
[20] Wang AF, Tang HY, Cao T, Salley SO, Ng KYS. J Colloid Interface Sci 2005;291:438.
[21] Chauhan AK, Aswal DK, Koiry SP, Gupta SK, Yakhmi JV, Sürgers C, Guerin D, Lenfant S, Vuillaume D. Appl Phys A 2008;90:581.
[22] Kim DH, Lee HS, Yang HC, Yang L, Cho K. Adv Funct Mater 2008;18:1363.
[23] Ling HF, Lin JY, Yi MD, Liu B, Li W, Lin ZQ, Xie LH, Bao Y, Guo FN, Huang W. ACS Appl Mater Interfaces 2016;8:18969.
[24] Tseng CW, Tao YT. J Am Chem Soc 2009;131:12441.
[25] Yi MD, Xie M, Shao YQ, Li W, Ling HF, Xie LH, Yang T, Fan QL, Zhu JL, Huang W. J Mater Chem C 2015;3:5220.
[26] Yu Y, Ma QH, Ling HF, Li W, Ju RL, Bian LY, Shi NE, Qian Y, Yi MD, Xie LH, Huang W. Adv Funct Mater 2019;29:1904602.
[27] Howarter JA, Youngblood JP. Langmuir 2006;22:11142.
[28] Yotphan S, Bergman RG, Ellman JA. Org lett 2010;12:2978.
[29] Pan ZH, Liu ML, Zheng CY, Gao DQ, Huang W. Chin J Chem 2017;35:1227.
[30] Wu HR, Zheng CY, Chen NW, Zhu J, Gao DQ. Tetrahedron Lett 2017;58:1576.
[31] Zhang H, Cai Q, Ma DW. J Org Chem 2005;70:5164.
[32] Kinarivala N, Trippier PC. Tetrahedron Lett 2014;55:5386.
[33] Zhong YN, Wang T, Gao X, Xu JL, Wang SD. Adv Funct Mater 2018;28:1800854.